# High temperature integrated ultrasonic shear and longitudinal wave probes

Ono, Y.; Jen, C.-K.; Kobayashi, M.

**Publisher's version / la version de l'éditeur:**
*Review of Scientific Instruments, 78, 2, pp. 024903-1-024903-5, 2007-02-01*

**Web page / page Web**
http://dx.doi.org/10.1063/1.2669719
http://nparc.cisti-icist.nrc-cnrc.gc.ca/npsi/ctrl?action=rtdoc&an=15782952&lang=en
http://nparc.cisti-icist.nrc-cnrc.gc.ca/npsi/ctrl?action=rtdoc&an=15782952&lang=fr

# High Temperature Integrated Ultrasonic Shear and Longitudinal Wave Probes

Y. Ono[a)], C.-K. Jen[b)], and M. Kobayashi[b)]

[a)] Department of Systems and Computer Engineering, Carleton University,
1125 Colonel By Drive, Ottawa, Ontario, K1S 5B6, Canada

[b)] Industrial Materials Institute, National Research Council of Canada,
75 Blvd. de Mortagne, Boucherville, Quebec, J4B 6Y4, Canada

(Received

**Abstract:**

Integrated ultrasonic shear wave probes have been designed and developed using a mode conversion theory for nondestructive testing and characterization at elevated temperatures. The probes consisted of metallic substrates and high temperature piezoelectric thick (> 40 μm) films through a paint-on method. Shear waves are generated due to mode conversion from longitudinal to shear waves because of reflection inside the substrate having a specific shape. A novel design scheme is proposed to reduce the machining time of substrates and thick film fabrication difficulty. A probe simultaneously generating and receiving both longitudinal and shear waves is also developed and demonstrated. In addition, a shear wave probe using a clad buffer rod consisting of an aluminum core and stainless steel cladding has been developed. All the probes were tested and successfully operated at 150 °C.

## 1. Introduction

Ultrasonic techniques are frequently used to carry out nondestructive testing and characterization (NDT&C) of materials and products due to their simplicity, speed, economy, safety, portability and capability to probe the interior of an opaque material.[1] Many NDT&C are also required to be performed at elevated temperatures, therefore high temperature (HT) ultrasonic transducers (UTs) are in demand. In addition, ultrasonic techniques prefer and sometimes need the UTs having large frequency bandwidth, strong signal and high signal-to-noise ratio (SNR). Various efforts have been devoted to the development of such piezoelectric HTUTs [2-5] and they may be supplied by several companies. However, the reported efforts have so far devoted to longitudinal (L) wave UTs only.

It is understood that shear (S) waves may be advantageous over L waves for NDT&C because liquid and gas media do not support S waves. For instance, the higher sensitivity to detect cracks or gaps filled with liquids could be expected using S waves than L waves in a ultrasonic pulse-echo technique since reflection coefficients of S waves at solid/liquid interfaces are unity, namely total reflection, while that of L waves are less than unity.[6] In addition, S waves have better spatial resolution than L waves to detect small defects such as cracks and inclusions in products and materials due to shorter wavelength of S waves than that of L waves at the same frequency.[6] Furthermore, for the evaluation of material properties, sometimes it is important to measure shear modulus and viscoelastic properties in which S wave properties are a requisite.[7]

A UT setup to generate and receive both L and S waves at the same sensor location and under the identical measurement conditions would be also of interest because engineering constants such as Young's modulus and Poisson's ratio require measurement of both S and L waves. In the past, special crystal cut, for instance, 10° rotated Y-cut lithium niobate and tilted *c*-axis zinc oxide thin films were reported to generate and receive both L and S waves simultaneously.[8] In this study, methods are presented to achieve HT integrated ultrasonic S wave probes and also provide a means to excite and receive both L and S waves at elevated temperatures.

## 2. Design using Mode Conversion Theory

The mode conversion from L to S waves due to reflection at an interface of two media, as shown in Fig. 1, was reported.[9,10] It means that the L wave UT together with L-S mode conversion caused by the reflection at a solid-air interface can generate S waves effectively and be used as a S wave probe.[11,12] In Fig. 1, incident $L_i$ waves generated by an L wave UT reach a solid-air interface with an incident angle of $\theta$ and reflected as $L_r$ and $S_r$ waves with a reflection angle of $\theta$ and $\varphi$, respectively. The equations governing the reflection and mode conversion are given in Eqs. (1)-(3),[9,11] where $V_l$ and $V_s$ are L and S wave velocities in the solid, respectively, $\sigma$ is Poisson's ratio of the solid, and $R_{ll}$ and $R_{sl}$ are energy reflection coefficients of the L and S waves, respectively.

$$\frac{V_s}{V_l} = \frac{\sin\varphi}{\sin\theta} = \sqrt{\frac{0.5-\sigma}{1-\sigma}} \tag{1}$$

$$R_{ll} = \left[\frac{\cos^2 2\varphi - \left(V_s/V_l\right)^2 \sin 2\theta \sin 2\varphi}{\cos^2 2\varphi + \left(V_s/V_l\right)^2 \sin 2\varphi \sin 2\theta}\right]^2 \tag{2}$$

$$R_{sl} = \frac{4\left(V_s/V_l\right)^2 \cos^2 2\varphi \sin 2\theta \sin 2\varphi}{\left[\cos^2 2\varphi + \left(V_s/V_l\right)^2 \sin 2\varphi \sin 2\theta\right]^2} \tag{3}$$

In order to investigate how much energy of $L_i$ waves are converted into S waves due to reflection, $R_{sl}$ were calculated with respect to $\theta$ with different $\sigma$ values in the range from 0 to 0.5 using Eqs. (1) and (3). The results are shown in Fig. 2 with a contour plot graph. The solid lines in Fig. 2 represent $\theta$ where the maximum $R_{sl}$ ($R_{sl\_max}$) is obtained for a given $\sigma$. From the result in Fig. 2 or by solving $R_{sl} = 1$ (or $R_{ll} = 0$), one can see that when $\sigma$ is smaller than 0.236, $R_{sl\_max}$ can be unity, which means that the $L_i$ waves are 100% converted into the S waves after reflection at these angles.[11] While

when $\sigma$ is larger than 0.263, $R_{sl}\_max$ monotonically decreases from 1 to 0 as $\sigma$ increases from 0.263 to 0.5.

### 2-1. Shear wave probe

Our design approach considers a simple way to fabricate S wave probes such that the L wave UT is in a plane parallel to the mode converted $S_r$ wave direction as shown in Fig. 3(a). This approach could reduce the machining time of the substrate and thick UT film fabrication difficulty. As considering this criterion, $\theta+\varphi$ needs to be 90°. The dashed line in Fig. 2 represents $\theta$ calculated by $\theta+\varphi = 90°$ and Eq. (1) at a given $\sigma$. One can see that $R_{sl}$ ($R_{sl}\_s$) at these $\theta$ are smaller than $R_{sl}\_max$ except at ($\theta$, $\sigma$) = (60°, 0.250) and (63.1°, 0.346) where the solid and dashed lines cross each other in Fig. 2. In order to compare $R_{sl}\_s$ with $R_{sl}\_max$, calculated $R_{sl}\_s$ and $R_{sl}\_max$ with respect to $\sigma$ are presented by the dashed and solid lines, respectively, in Fig. 4. The difference $R_{sl}\_max$–$R_{sl}\_s$ is shown by the dotted line in Fig. 4 as well. It is found that the differences are less than 0.01 in the $\sigma$ range between 0.224 and 0.382. It is noted that $\sigma$ of typical metallic materials of our interest for high temperature substrates, such as a mild steel ($\sigma$ = 0.29), stainless steel (0.30), inconel (0.31), magnesium (0.32), titanium (0.32) and aluminum (0.355), are within this range of $\sigma$.[13]

### 2-2. Shear and longitudinal wave probe

If one needs to generate and receive both L and S waves at the same time, then the S wave probe shown in Fig. 3(a) can be modified to achieve such a purpose. It simply makes a slanted surface with an angle 45° from the intersection of the slanted plane and the line from the center of the L UT as shown in Fig. 3(b). The 45° angle plane will reflect the energy of the $L_i$ wave into the $L_{r,45°}$ wave normal to the probing end as shown in Fig. 3(b). Therefore, in principle, the upper part of the $L_i$ waves, generated by the L UT, can be used to produce the $S_r$ waves and the lower part to produce the $L_{r,45°}$ waves.

## 3. Fabrication and Performance

We have developed integrated L wave thick (> 40 μm) piezoelectric film HTUTs.[4] Thick ceramic films as piezoelectric UTs can be deposited onto metallic and non-metallic substrates by a spray technique. In the film fabrication, a composite consisting of piezoelectric powders such as lead-zirconate-titanate (PZT) or bismuth titanate (BIT) well mixed with solution such as PZT of high dielectric constant is directly sprayed onto the substrate. The detailed fabrication procedure of the HTUTs was published elsewhere.[4] The attractive characteristics of these L UTs are that: they (a) can be integrated onto desired planar or curved substrates at desired NDT&C sites with handheld equipment and under possible lowest temperature without a furnace; (b) do not need a couplant; (c) can operate in pulse-echo and transmission modes with a SNR better than 30 dB between 5 and 10 MHz; (d) can operate from –100 °C up to more than 400°C; and (e) can operate with an array configuration. Such integrated L wave HTUTs together with the above mentioned characteristics are used to achieve our HT integrated ultrasonic S wave and L wave probes presented here.

### 3-1. Shear wave probe

Figure 5 shows a HT integrated ultrasonic S wave probe developed. The substrate material employed was an aluminum having $\sigma = 0.355$.[13] From the results in Figs. 2 and 4, $\theta$ was obtained 64.63° with $R_{sl\_s} = 0.7534$. Therefore, the energy conversion rate from the $L_i$ waves to the $S_r$ waves is 75.34 %, which is only 0.06% smaller than the maximum conversion rate with $R_{sl\_max} = 0.7540$ at $\theta =$ 63.53°. An L wave HTUT with a PZT composite was fabricated on a plane normal to the surface of the probing end as shown in Figs. 3(a) and 5. Typically, the measured piezoelectric coefficient $d_{33}$ of this PZT composite film is about 30 x $10^{-12}$ m/V, the electromechanical coupling coefficient $K_t$ about 0.2, the relative dielectric constant 320, the density 4400 kg/m$^3$ and the L wave velocity about 2200 m/s. A top

electrode was formed on the PZT composite film using a silver paste. The aluminum substrate serves as a bottom electrode.

Figures 6(a) and 6(b) show the ultrasonic signals in time and frequency domain, respectively, of the received $S_r$ waves in the pulse-echo mode at 150 °C. $S^n$ (n = 1,2...) represents nth round trip of the $S_r$ wave echoes traversing back and forth between the L UT and the probing end in Figs. 3(a) and 5. The $S_r$ waves reflected from the probing end were converted back to the L waves due to reflection at the slanted plane and received with the L UT. The center frequency of the $S^1$ echo was 6.1 MHz and the 6 dB bandwidth was 5.2 MHz. The SNR of $S^1$ echo was 36 dB. The SNR is defined as the ratio of the amplitude of the $S^1$ echo over that of the undesired signals between the $S^n$ echoes in Fig. 6(a). The signal strength of the $S^1$ echo at 150 °C was 4 dB smaller than that at room temperature. It can be seen that the received $L_r$ wave is not visible due to the fact that the dimension of the substrate has been chosen such that the reflected $L_r$ wave does not enter into the L UT effectively. It is noted that the UT can operate at temperatures higher than 400 °C when BIT powders instead of PZT powders are used .[4,5] Indeed, the same design scheme has been also applied onto a mild steel substrate with a HTUT using a BIT composite film and ultrasonic performance with good SNR has been obtained at 300°C.

### 3-2. Shear and longitudinal wave probe

Figure 7 presents a HT integrated ultrasonic S and L wave probe developed. An additional 45° angle plane with respect to the L wave UT was machined onto the S wave probe in Fig. 5, based on the probe design shown in Fig. 3(b). Figure 8 (a) shows ultrasonic signals in time domain in the pulse-echo mode at 150 °C, in which the $S_r$ ($S^1$) and $L_{r,45°}$ ($L^1$) waves are observed simultaneously. The $L^1$ represents the first round trip L wave echo traversing between the L UT and the probing end. During the top electrode fabrication for the probe shown in Fig. 7, the area of the top electrode was adjusted so that the amplitude of the reflected $S_r$ and $L_{r,45°}$ waves were nearly the same. The SNR of the $L^1$ and $S^1$ were both 18 dB. The center frequencies of the $L^1$ and $S^1$ echoes were 6.9 MHz and 5.7 MHz and the 6 dB

bandwidths were 8.1 MHz and 5.7 MHz, respectively, as shown in Fig. 8(b). The center frequency of the $S^1$ echo was 1.2MHz lower than that of the $L^1$ echo because of larger attenuation of high frequency components of S waves than those of L waves. As expected, the frequency spectra of the converted S waves are almost identical in Fig. 6(b) and Fig. 8(b). The similar approach was also applied onto a mild steel substrate with the BIT HTUT and ultrasonic measurement results at 300 °C with good SNR were also obtained.

### 3-3. Clad buffer rod probe

For ultrasonic NDT&C at elevated temperatures, buffer rods are often used to keep UTs away from high temperature in order to prevent the UTs from their thermal damage.[14] A probing end of the buffer rod contacts high temperature materials while another UT end is cooled so that the UT can safely operate. However, the well-known problem using a long buffer rod in the pulse-echo mode is the presence of spurious echoes (trailing echoes) due to mode conversion, wave reverberation and diffraction within the rod of finite diameter and specific shape.[15,16] The spurious echoes also involve scattering echoes from random grains or voids in the rod materials. The spurious signals are unwanted since they deteriorate the SNR of the probe. In order to improve the SNR, ultrasonic clad-buffer rods consisting of a metallic core and a metallic cladding were developed.[17] We have also attempted to develop a HT integrated clad buffer rod ultrasonic S wave probe.

Figure 9 shows a HT clad buffer rod S wave probe developed. The buffer rod consisted of aluminum core and stainless steel (SS) cladding. A cross-sectional dimension of the aluminum core was 23 mm by 23 mm and the length was about 120 mm. The SS cladding with a thickness of 1-2 mm was formed onto the side faces of the aluminum core using a thermal spray technique.[17] No cladding was formed onto the probing end, the slanted surface and the area where the L UT was fabricated. An L wave HTUT with a PZT composite was fabricated on a plane normal to the surface of the probing end as shown in Fig. 9. Figures 10(a) and (b) show the ultrasonic signals in time and frequency domain,

respectively, of the received $S_r$ wave in the pulse-echo mode at 150 °C. The center frequency of the $S^1$ echo was 4.7 MHz and the 6 dB bandwidth was 2.2 MHz. The SNR of $S^1$ echo was 25 dB and the trailing echoes were not visible thanks to the SS cladding layer.[17] With this design of the clad buffer rods, the probes can be applicable to NDT&C at temperatures much higher than the maximum operating temperature of the UT employed together with a cooling system attached onto the buffer rod.

**4. Conclusions**

Ultrasonic S wave probes were designed using metallic substrates with the use of mode conversion from L to S waves. A novel approach was taken to fabricate the L wave UT and let the L UT be in a plane parallel to the propagation direction of the mode converted S waves. Theoretical calculation of the energy conversion rate from the L to S waves due to reflection indicates that the differences between $R_{sl}\_s$ with the proposed design and $R_{sl}\_max$ are less than 1% in the $\sigma$ range between 0.224 and 0.382 with which many of metallic substrates, such as mild steel, stainless steel, inconel, magnesium, titanium and aluminum, of our interest for high temperature probes are affiliated. This novel design approach could reduce the machining time of substrates and thick film fabrication difficulty.

A HT integrated ultrasonic S wave probe has been fabricated using an aluminum substrate based on the design proposed. A piezoelectric thick (> 40μm) film HTUT with a PZT composite was attached onto the substrate through a paint-on method. A probe that can simultaneously generate and receive both L and S waves has been also developed and demonstrated. Furthermore, an S wave probe using a clad buffer rod consisting of an aluminum core and a SS cladding has been developed. All the above mentioned probes were tested and successfully operated up to 150 °C with a center frequency of 5–7 MHz, 6dB bandwidth of 2–8 MHz, and SNR of better than 18 dB. It is noted that the UT can operate at temperatures higher than 400 °C when BIT powders instead of PZT powders as a piezoelectric material

are used.[4,5] The same design scheme has been applied onto a mild steel substrate with the BIT HTUTs and ultrasonic performance with good SNR has been obtained at 300°C.

**Acknowledgments**

Authors would like to thank K.-T. Wu and H. Hebert for their technical assistance. Financial support from Natural Sciences and Engineering Research Council of Canada is acknowledged.

**References:**


[1] J. Krautkrämer and H.H. Krautkrämer, Ultrasonic Testing of Materials (Springer-Verlag, Berlin, 1990).

[2] T. Arakawa, K. Yoshikawa, S. Chiba, K. Muto, and Y Atsuta, Nondestr. Test. Eval. 7, 263 (1992).

[3] K.J. Kirk, A. McNab, A. Cochran, I. Hall, and G. Hayward, IEEE Trans. Ultrason. Ferroelect. Freq. Contr. **46**, 311 (1999).

[4] M. Kobayashi and C.-K. Jen, Smart Mat. and Structures **13**, 951 (2004).

[5] R. Kazys, A. Voleisis, R. Sliteris, L. Mazeika, R.V. Nieuwenhove, P. Kupschus, and H.A. Abderrahim, IEEE Trans. Ultrason. Ferroelect. Freq. Contr. **52**, 525 (2005).

[6] H. Kuttruff, Ultrasonics Fundamentals and Applications (Elsevier Applied Science, London, 1991), pp. 277-279.

[7] W.P. Mason, W.O. Baker, H.J. McSkimin, and J.H. Heiss, Physical Review **75**, 936 (1949).

[8] C.-K. Jen, K. Sreenivas, and M. Sayer, J. Acoust. Soc. Am. **84**, 26 (1988).

[9] W.G. Mayer, Ultrasonics **3**, 62 (1965).

[10] B.A. Auld, Acoustic Fields and Waves in Solids **2** (John Wiley & Sons, New York, 1973), pp. 30-38.

[11] G.S. Kino, Acoustic Waves, Devices, Imaging & Analog Signal Processing, (Prentice-Hall, New Jersey, 1987), Chap. 2, pp. 85-153.

[12] M.O. Si-Chaib, H. Djelouah, and M. Bocquet, NDT&E International **33**, 91 (2000).

[13] A.R. Selfridge, IEEE Trans. on Sonics and Ultrason. **SU-32**, 381 (1985).

[14] L.C. Lynnworth and V. Magori, in Physical Acoustics, edited by R.N. Thurston, A.D. Pierce, and E.P. Papadakis, **XXIII** (Academic, New York, 1999), pp. 275-470.

[15] M. Redwood, Mechanical Waveguides, (Pergamon, New York, 1960), pp. 190-207.

[16] C.-K. Jen, L. Piche, and J.F. Bussiere, J. Acoust. Soc. Amer. **88**, 23 (1990).

[17] C.-K. Jen, J.-G. Legoux, and L. Parent, NDT & E Int. **33**, 145 (2000).

**Figure Captions:**

Fig. 1 Reflection and mode conversion with an incidence of L wave at a solid-air interface.

Fig. 2 Energy reflection coefficients $R_{sl}$ with respect to L wave incident angle $\theta$ with different Poisson's ratio $\sigma$. Solid and dashed lines represents $\theta$ at which maximum $R_{sl}$ ($R_{sl\_max}$) is obtained and at which $\theta + \varphi$ equals to 90° for a given $\sigma$, respectively, where $\varphi$ is the reflection angle of S waves.

Fig. 3 Schematic diagrams of (a) S wave and (b) S and L wave probes.

Fig. 4 Energy reflection coefficients $R_{sl\_max}$ (solid line) and $R_{sl\_s}$ (dashed line) with respect to $\sigma$ obtained from the results represented by the solid and dashed line, respectively, in Fig. 2. Dotted line represents the difference $R_{sl\_max} - R_{sl\_s}$.

Fig. 5 A HT integrated ultrasonic S wave probe with the L wave UT located in a plane parallel to the direction of mode converted $S_r$ waves, where $\theta = 64.6°$.

Fig. 6 Ultrasonic signals of mode converted $S_r$ ($S^n$) waves in (a) time and (b) frequency domain obtained using the S wave probe shown in Fig. 5 with a pulse-echo technique at 150 °C. $S^n$ (n=1,2…) denotes nth round trip of the $S_r$ wave echoes traveling between the L UT and probing end in Figs. 3(a) and 5.

Fig. 7 A HT integrated ultrasonic S and L wave probe. An additional 45° angle plane with respected to the L UT was machined onto the S wave probe shown in Fig. 5.

Fig. 8 Ultrasonic signals in (a) time and (b) frequency domain of $S_r$ ($S^1$) and $L_{r,45°}$ ($L^1$) waves at 150°C obtained using the S and L wave probe in Fig. 7.

Fig. 9 An integrated S wave probe using clad buffer rod consisting of aluminum core and stainless steel cladding.

Fig. 10 Ultrasonic signals in (a) time and (b) frequency domain of the $S_r$ waves obtained using the clad buffer rod S wave probe shown in Fig. 9 at 150 °C.

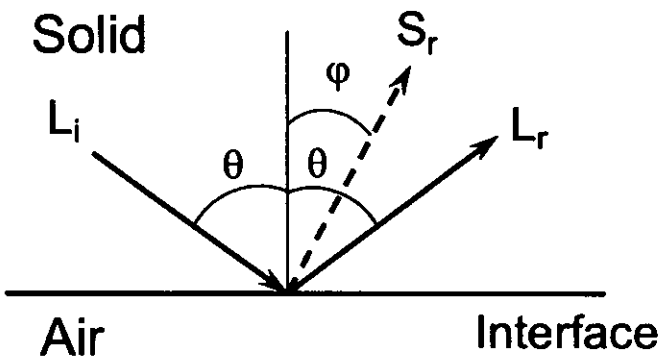


Fig. 1

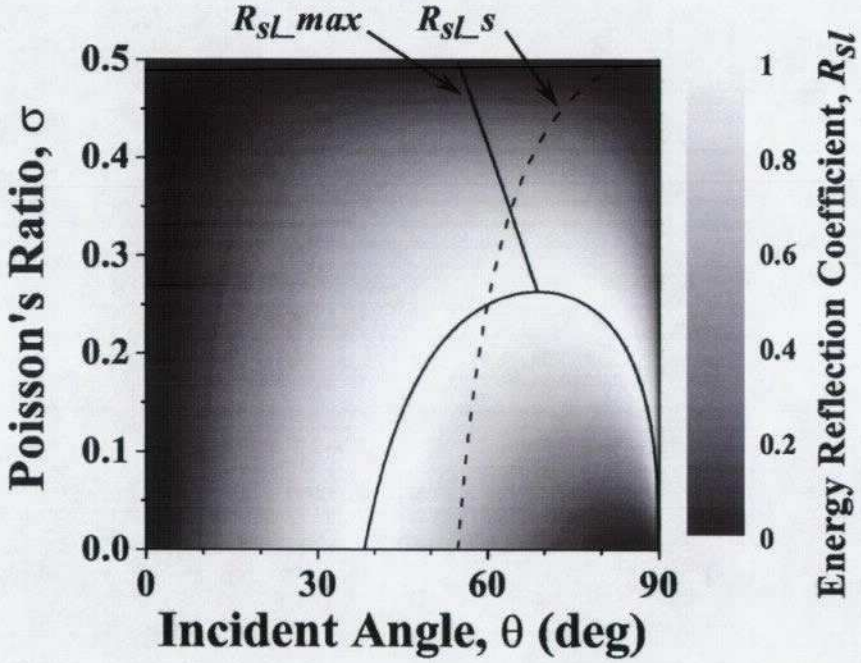
$R_{sL\_max}$
$R_{sL\_s}$
Poisson's Ratio, σ
0.5
0.4
0.3
0.2
0.1
0.0
0
30
60
90
Incident Angle, θ (deg)
1
0.8
0.6
0.4
0.2
0
Energy Reflection Coefficient, $R_{sl}$

Fig. 2

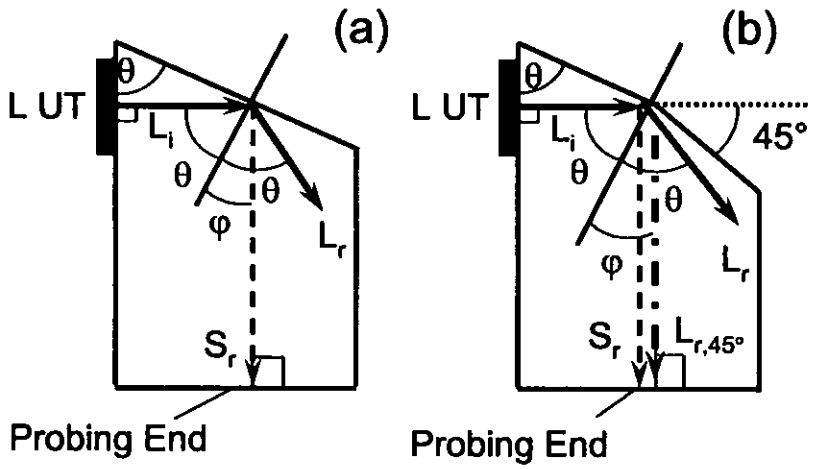
(a)
L UT
θ
$L_i$
θ
θ
φ
$L_r$
$S_r$
Probing End
(b)
L UT
θ
$L_i$
θ
θ
45°
φ
$L_r$
$S_r$
$L_{r,45°}$
Probing End

Fig. 3

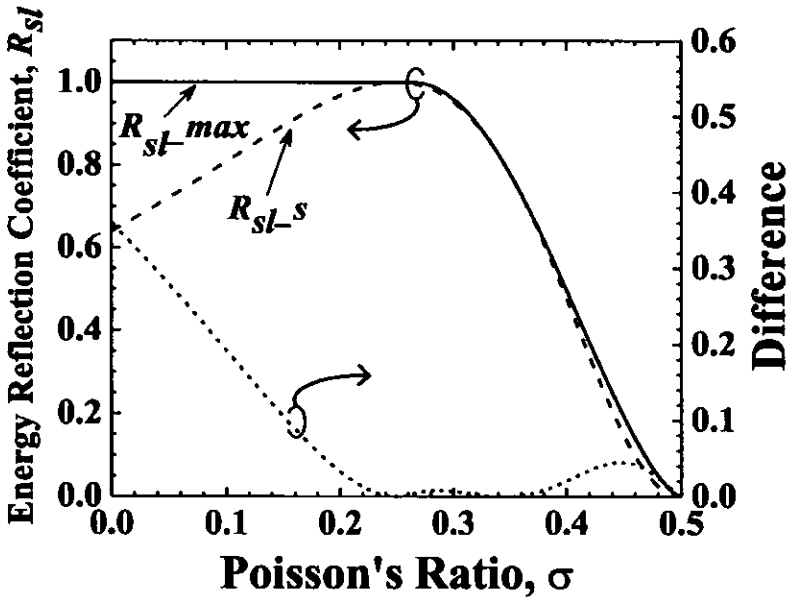
Energy Reflection Coefficient, $R_{sl}$
Difference
Poisson's Ratio, σ
$R_{sl\_max}$
$R_{sl\_s}$
1.0
0.8
0.6
0.4
0.2
0.0
0.6
0.5
0.4
0.3
0.2
0.1
0.0
0.0
0.1
0.2
0.3
0.4
0.5

Fig. 4

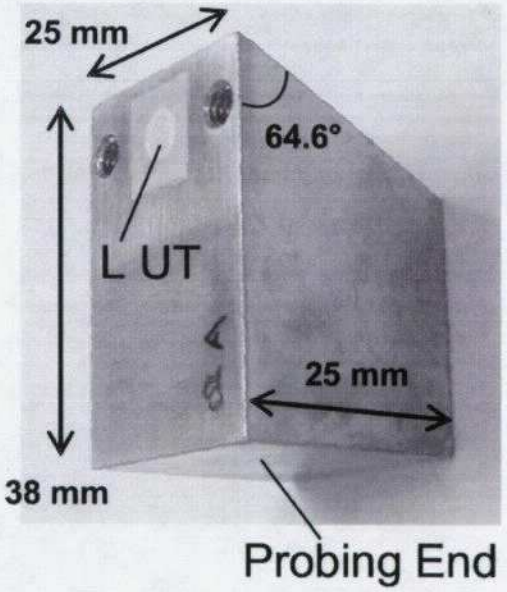


Fig. 5

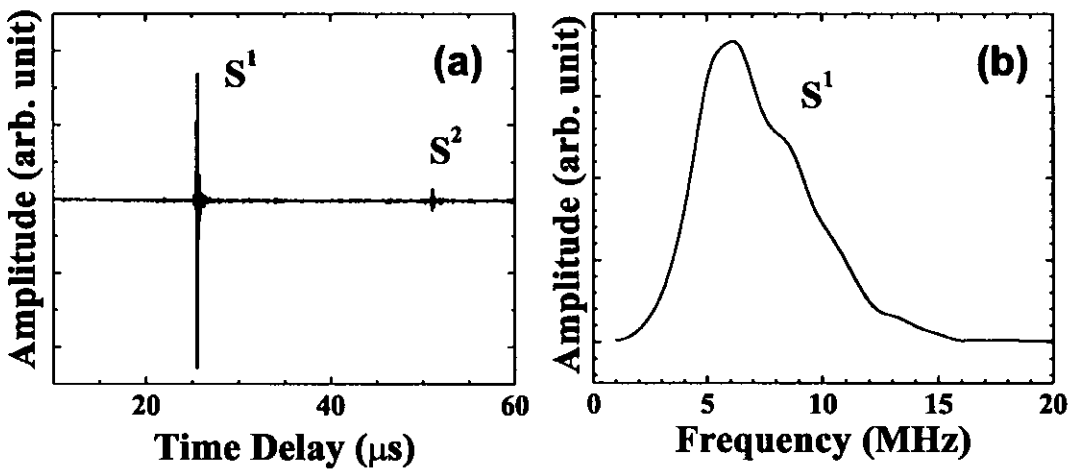
Amplitude (arb. unit)
S1
(a)
S2
20
40
60
Time Delay (μs)
Amplitude (arb. unit)
S1
(b)
0
5
10
15
20
Frequency (MHz)

Fig. 6

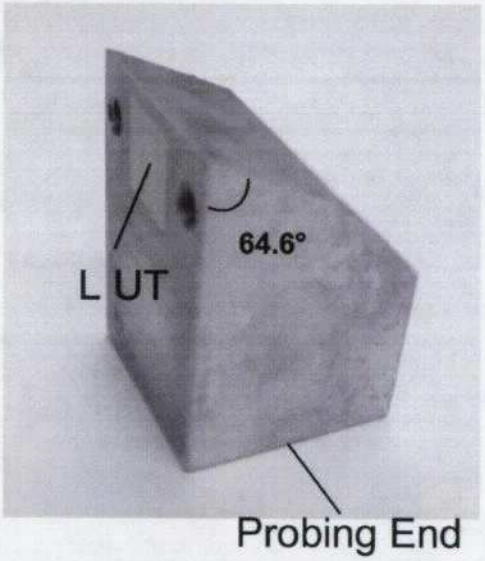


Fig. 7

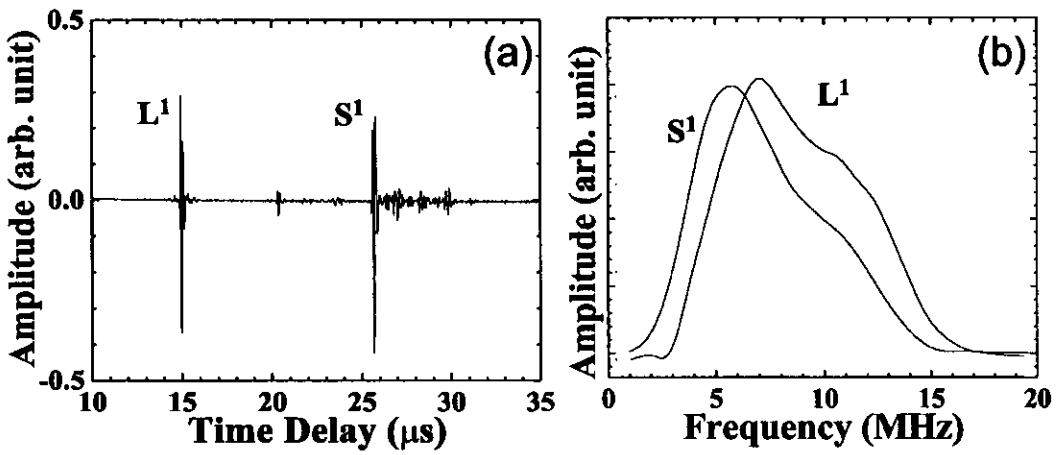
(a)
L1
S1
0.5
0.0
-0.5
Amplitude (arb. unit)
10
15
20
25
30
35
Time Delay (μs)
(b)
S1
L1
Amplitude (arb. unit)
0
5
10
15
20
Frequency (MHz)

Fig. 8

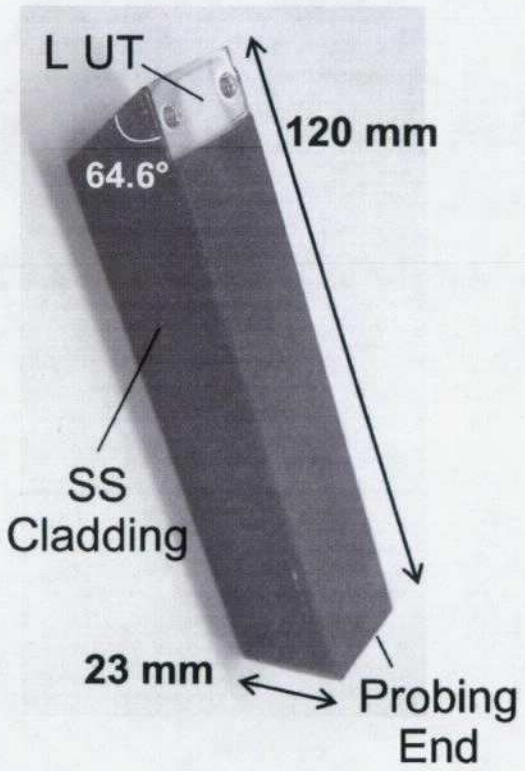


Fig. 9

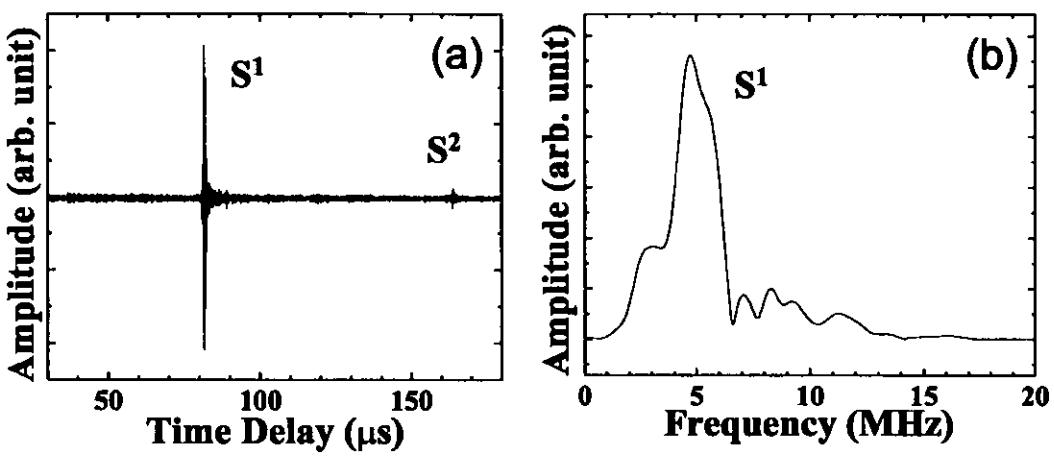
Amplitude (arb. unit)
S1
(a)
S2
50
100
150
Time Delay (μs)
Amplitude (arb. unit)
S1
(b)
0
5
10
15
20
Frequency (MHz)

Fig. 10